Journal of Solid State Chemistry **165,** 363–371 (2002)
doi:10.1006/jssc.2002.9552, available online at http://www.idealibrary.com on IDEAL®

Crystal Structures and Ionic Conductivities of Ternary Derivatives of the Silver and Copper Monohalides

I. Superionic Phases of Stoichiometry MA_4I_5: $RbAg_4I_5$, KAg_4I_5, and KCu_4I_5

S. Hull,*,[1] D. A. Keen,*,† D. S. Sivia,* and P. Berastegui‡

*The ISIS Facility, Rutherford Appleton Laboratory, Chilton, Didcot, Oxon OX11 0QX, United Kingdom; †Physics Department, Oxford University, Clarendon Laboratory, Parks Road, Oxon OX1 3PU, United Kingdom; and ‡Arrhenius Laboratory, Stockholm University, S-106 91 Stockholm, Sweden

Received September 28, 2001; in revised form February 19, 2002; accepted February 22, 2002

The superionic properties of the compounds $RbAg_4I_5$, KAg_4I_5 and KCu_4I_5 have been investigated by powder neutron diffraction and complex impedance spectroscopy. $RbAg_4I_5$ and KAg_4I_5 have room-temperature ionic conductivities of $\sigma = 0.21(6)$ and $0.08(5)$ $\Omega^{-1}\,cm^{-1}$, respectively, which increase gradually on increasing temperature. KCu_4I_5 is only stable in the temperature range between 515(5) K and its melting point of 605 K, and its ionic conductivity is $\sigma = 0.61(8)$ $\Omega^{-1}\,cm^{-1}$, at $T = 540$ K. At lower temperatures, KCu_4I_5 disproportionates into KI + 4CuI and the ionic conductivity falls by over three orders of magnitude. Least-squares refinements of the powder neutron diffraction data for $RbAg_4I_5$ at ambient temperature confirm the reported structure (space group $P4_132$, $Z = 4$, $a = 11.23934(3)$ Å), though with some differences in the preferred locations of the mobile Ag^+. KAg_4I_5 and KCu_4I_5 are found to adopt the same basic structure as $RbAg_4I_5$, with the I^- forming a β-Mn-type sublattice, with the K^+ located in a distorted octahedral environment and the $Ag^+(Cu^+)$ predominantly distributed over two sites which are tetrahedrally co-ordinated to I^-. The implications for the conduction mechanism within these compounds are discussed, using a novel maximum entropy difference Fourier technique to map the distribution of the $Ag^+(Cu^+)$ within the unit cell. © 2002 Elsevier Science (USA)

Key Words: **superionic conduction; Ag^+ diffusion; neutron diffraction; maximum entropy techniques.**

1. INTRODUCTION

The superionic properties exhibited by silver iodide, AgI, at temperatures above 420 K have encouraged a number of studies of the binary phase diagrams of the type AgI–*M*I, where *M* is one of the alkali metals K^+, Rb^+ and Cs^+ (1–4). These are principally aimed at identifying ternary compounds with lower values of superionic transition temperature and (with an eye to potential technological applications within solid-state batteries) preferably to lower than ambient. The continued interest in solids with high ionic conductivities has motivated a re-examination of these systems by the authors, using powder neutron diffraction and impedance spectroscopy methods.

In the case of the AgI–KI system, Bradley and Greene identified two compounds, K_2AgI_3 and KAg_4I_5 (1). The former is stable up to ~400 K but is a poor conductor. KAg_4I_5 was found to be stable over the temperature range from 311 K to its congruent melting point of 526 K and possesses a high value of ionic conductivity ($\sigma \sim 0.31$ $\Omega^{-1}\,cm^{-1}$ at 520 K (1)). Transport measurements confirmed that the current is carried by Ag^+ ions and KAg_4I_5 could be retained for several hours at ambient temperature in a dry atmosphere, before undergoing disproportionation to β-AgI and K_2AgI_3. Subsequently, a comprehensive study of the AgI–*M*I systems by the same authors (2) (plus the analogous AgBr–*M*Br and CuI–*M*I cases) identified a KCu_4I_5 compound stable from 530 to 605 K and, most interestingly, $RbAg_4I_5$ which is stable at ambient temperature with $\sigma = 0.124(6)$ $\Omega^{-1}\,cm^{-1}$. No analogous bromides were found and later studies failed to synthesize a chloride of stoichiometry KAg_4Cl_5 (5). The compound $RbCu_4I_5$ was not observed, though partial replacement of I^- by Cl^- to compensate for the small size of the Cu^+ was found to stabilize a highly conducting compound $RbCu_4Cl_3I_2$ (6, 7) at ambient temperature.

The exceptionally high ionic conductivity of $RbAg_4I_5$ has encouraged many diverse studies of its physical properties (8–15), including investigations of the Ag^+ conduction mechanism (16, 17) and two low-temperature phase transitions (18). At ambient temperature, its crystal structure was determined to be cubic, with a lattice parameter $a \sim 11.24$ Å (8, 9). The space group was assigned to one of the enantiomorphic pair $P4_132$ (9) and $P4_332$ (8). In this arrangement, the I^- sublattice approximates to that adopted by the atoms in the β-Mn structure and the Rb^+ are co-ordinated to six anions. The $16 \times Ag^+$ ions per unit cell

[1] To whom the correspondence should be addressed. Fax: + 44-1235-445720. E-mail: s.hull@rl.ac.uk.

0022-4596/02 $35.00

were distributed in different ways over 60 (9) or 72 (8) different sites. These positions will be discussed in more detail in Section 3. However, to the best of our knowledge, no diffraction studies of the two related compounds KAg_4I_5 and KCu_4I_5 have been reported, presumably because structural studies within their stability fields requires the use of high-temperature methods. In this paper, we report the ionic conductivity and crystal structures of the three compounds $RbAg_4I_5$, KAg_4I_5 and KCu_4I_5, using impedance spectroscopy and powder neutron diffraction methods. Implications for the likely conduction mechanisms are presented.

2. EXPERIMENTAL

The polycrystalline samples were prepared from stoichiometric mixtures of the binary halides AgI, CuI, RbI and KI of stated purities 99.999, 99.999, 99.975 and 99.99%, respectively. $RbAg_4I_5$ was prepared by sealing the mixture in a gold crucible and heating to 510 K for 48 h. The resultant white powder was kept in a dry atmosphere prior to and between measurements. KAg_4I_5 is not stable at ambient temperature and was, therefore, prepared immediately before the experiments by heating a KI + 4AgI mixture under vacuum to 500 K for 24 h. Diffraction studies showed that the compound is stable for at least one day if kept in a dry atmosphere. KCu_4I_5 cannot be retained at temperatures below 515(5) K and the appropriate mixture was sealed in a thin-walled silica ampoule of 6 mm diameter and 44 mm length.

The powder neutron diffraction studies were performed on the Polaris powder diffractometer at the ISIS facility, UK (19). Data were collected using the backscattering detector bank ($135^\circ < \pm 2\theta < 160^\circ$, d-spacing range $0.5 < d$ (Å) < 3.2 and resolution $\Delta d/d \sim 5 \times 10^{-3}$) and were corrected for the effects of neutron absorption by the sample and analyzed using the least-squares Rietveld refinement program TF12LS (20), which is based on the Cambridge Crystallographic Subroutine Library (21). Data collected at temperatures close to ambient ($RbAg_4I_5$ and KAg_4I_5) were performed with the powders inside thin-walled vanadium sample cans of 11 mm diameter. High-temperature measurements were performed with the samples (sealed in silica) heated inside a furnace designed for neutron diffraction constructed using vanadium foil resistive heating element and heat shields. The quality of the fits was assessed using the usual goodness-of-fit χ^2 statistic, defined by

$$\chi^2 = \sum_{N_d} \frac{(y_{obs} - y_{calc})^2}{(\sigma y_{obs})^2} (N_d - N_v).$$

N_d is the number of data points used in the fit and N_v is the number of fitted variables. I_{obs} and I_{calc} are the observed and calculated intensities, respectively, and σI_{obs} is the estimated standard deviation on I_{obs}, derived from the counting statistics.

Measurements of the ionic conductivity were performed using pelleted samples of ~ 5 mm diameter and ~ 5 mm length. The samples were heated at 0.5 K min^{-1} to temperatures of 466(2) K ($RbAg_4I_5$), 454(2) K (KAg_4I_5) and 540(2) K (KCu_4I_5), these being chosen with reference to the phase diagrams reported previously (1–4). All measurements were performed under dynamic vacuum of $< 10^{-4}$ bar. Complex impedance and admittance data were collected over the frequency range 10^{-1}–10^7 Hz using a Solartron S1260 Frequency Response Analyser and analyzed using in-house software (22) to determine the sample resistance and, hence, the ionic conductivity σ. The data for σ versus T were found to be reproducible after the first heating/cooling cycle (presumably due to sintering of the pellet on first heating and mixing of KI + 4AgI in the case of KAg_4I_5) and data collected on the second heating/cooling cycle are presented here.

3. RESULTS

Figure 1 shows the ionic conductivity of $RbAg_4I_5$ and KAg_4I_5 versus temperature. At ambient temperature, their ionic conductivities are $\sigma = 0.21(6)$ and $0.08(5)\,\Omega^{-1}\,cm^{-1}$, respectively, in good agreement with the values presented previously (1, 2). $RbAg_4I_5$ is a slightly better ionic conductor than KAg_4I_5 over the entire temperature range, probably because Rb^+ is larger than K^+ and the resultant expansion of the lattice makes Ag^+ diffusion through any bottlenecks within the anion sublattice easier. Their ionic conductivity values do not increase rapidly with temperature and there is no evidence of any discontinuity in the trace for KAg_4I_5 at its lower stability limit of $T \sim 311$ K because the sample is under dynamic vacuum and no significant disproportionation takes place over the time scale of the measurements. As illustrated in Fig. 1, the formation of KCu_4I_5 is characterized by an increase in the ionic conductivity by $\sim 10^3\times$, reaching a value of $\sigma = 0.61(8)\,\Omega^{-1}\,cm^{-1}$ at $T = 540$ K. Figure 2 shows the neutron diffraction data collected for the KI + 4CuI mixture on cooling from 594 K. At 514(5) K, there is an abrupt change in the diffraction pattern, illustrating the disproportionation of the high-temperature KCu_4I_5 phase to the constituent halides. In particular, there is no evidence of phases of intermediate stoichiometry (unlike its Ag^+ analogue, which disproportionates by $2KAg_4I_5 \rightarrow 7AgI + K_2AgI_3$ (1)).

The crystal structure of $RbAg_4I_5$ has been reported previously (8, 9) using cubic space group $P4_132$ or its enantiomorph $P4_332$. The former is chosen here. The cubic lattice parameter is $a = 11.24$ Å, such that there are four formula units within the unit cell. The anions are distributed over two sites, labelled I1 (in 8(c) x,x,x sites with $x \sim 0.03$)

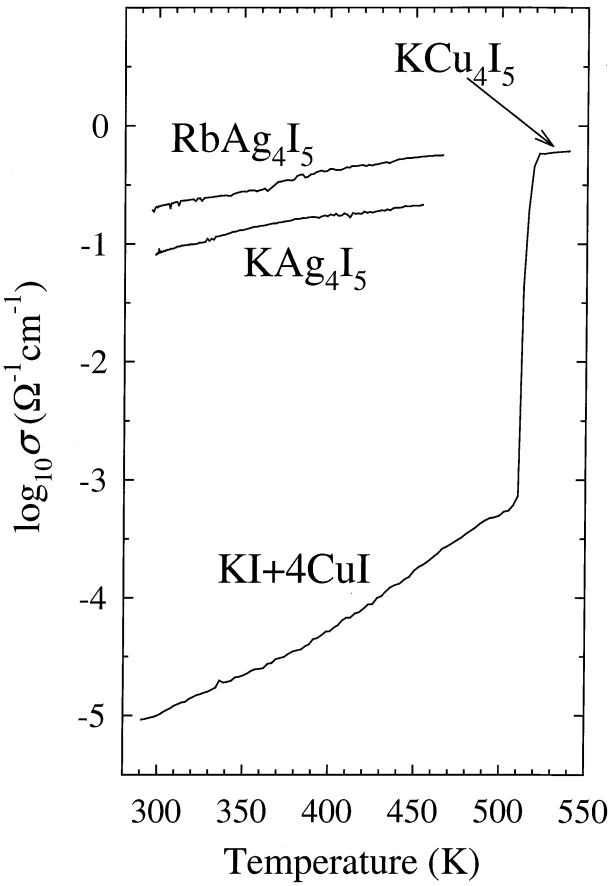

FIG. 1. The temperature variation of the ionic conductivity $\log_{10}\sigma$ for $RbAg_4I_5$, KAg_4I_5 and KCu_4I_5. The disproportionation of the KCu_4I_5 into KI + 4CuI on cooling at 515(5) K results in a drop in σ of over three orders of magnitude.

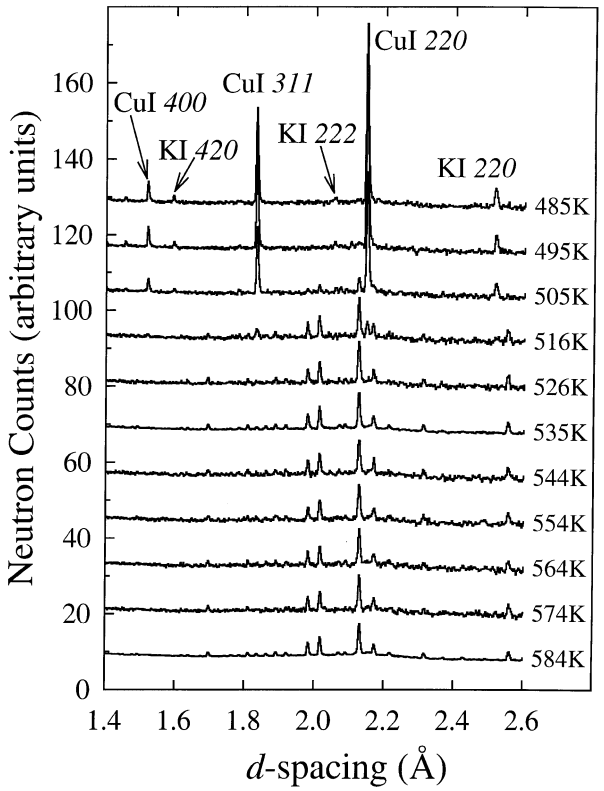

FIG. 2. The evolution of a portion of the powder neutron diffraction pattern collected from KCu_4I_5 on cooling, showing the disproportionation to form CuI + 4KI at around 510 K.

and I2 (in 12(*d*) $\frac{1}{8},y,\frac{1}{4}-y$ sites with $y \sim 0.18$). The $4\times Rb^+$ are located in the 4(*a*) $\frac{3}{8},\frac{3}{8},\frac{3}{8}$ sites. The locations of the $16\times Ag^+$ per unit cell have been the subject of some discussion within the literature. Geller (9) found that these were predominantly located in two sets of general 24(*e*) positions, with $x \sim 0.53$, $y \sim 0.27$, $z \sim 0.80$ and $x \sim 0.99$, $y \sim 0.85$, $z \sim 0.22$. We label these as Ag1 and Ag2 sites, respectively. Small, though significant, occupancies were also found for the 8(*c*) *x*,*x*,*x* sites with $x \sim 0.17$ (Ag3) and the 4(*b*) $\frac{7}{8},\frac{7}{8},\frac{7}{8}$ sites (Ag4). Bradley and Greene (8) also considered the above sites, plus a fifth (Ag5) in 12(*d*) $\frac{1}{8},y,\frac{1}{4}-y$ with $y \sim 0.80$, but suggested that the Ag^+ were randomly distributed over all 72 sites ($24\times Ag1 + 24\times Ag2 + 8\times Ag3 + 4\times Ag4 + 12\times Ag5$) with equal probability.

The observed Bragg peaks from $RbAg_4I_5$ at ambient temperature are consistent with a primitive cubic unit cell of dimension $a \sim 11.24$ Å. To confirm this, we initially performed a so-called 'model independent' least-squares fit to the diffraction data, which varies the 15 coefficients of a polynomial describing the background (diffuse) scattering, the unit cell parameter *a*, a Gaussian peak width parameter and the intensities of the Bragg peaks at *d*-spacings allowed by space group $P4_132$. This procedure follows that first proposed by Pawley (23) and does not impose (or provide) any direct structural information concerning the time-averaged location of the ions within the unit cell but it confirms the assignment of the unit cell and space group. In addition, the value of χ^2 obtained ($\chi^2 = 1.32$) gives an estimate of the lowest value that can reasonably be obtained using a structural model and also gives the intensities of the various Bragg peaks which will subsequently be used to generate difference Fourier maps of the ionic density.

To investigate the ionic arrangement within $RbAg_4I_5$, the diffraction data were initially fitted using a simplified structural model including the Rb, I1 and I2 sites described above and with the Ag^+ distributed equally over the Ag1 and Ag2 sites found to be predominantly occupied by Geller (9). The variable parameters were then an overall scale factor, a Gaussian peak width parameter, 15 coefficients of a background polynomial, eight positional parameters (x_{I1}, y_{I2}, x_{Ag1}, y_{Ag1}, z_{Ag1}, x_{Ag2}, y_{Ag2} and z_{Ag2}) and four isotropic temperature factors (B_{Rb}, B_{I1}, B_{I2} and B_{Ag} ($= B_{Ag1} = B_{Ag2}$)). This gave a relatively good fit to the data with $\chi^2 = 2.03$. The fraction of Ag^+ was next allowed to vary over the Ag1 and Ag2 sites (occupancies m_{Ag1} and m_{Ag2}) and then further

allowed to redistribute over the Ag3 site as well (with the additional positional parameter x_{Ag3}). This led to a slight improvement in χ^2 to 1.86. In these cases, the total Ag^+ content in the unit cell was always constrained to the value 16 predicted by the chemical formula. Inclusion of the Ag4 and Ag5 sites did not significantly improve χ^2 and the values of their site occupancies were (within error) zero. As a result, these sites were not considered further. Removal of the constraint on the thermal vibration parameters (i.e., allowing $B_{Ag1} \neq B_{Ag2} \neq B_{Ag3}$) reduced χ^2 to a value of 1.77, though the occupancy of the Ag3 site fell to a rather small value. This value of χ^2 is still slightly higher than that provided by the model independent fit, indicating that the structural model adopted is a close, but not exact, representation of the true structure. Attempts to improve the quality of the fit using anisotropic thermal vibration parameters for Rb, I1 and I2 produced small, yet significant, improvements in χ^2 (to 1.53). Allowing the thermal vibrations of the Ag^+ to become anisotropic produced a small reduction in χ^2, though the fit was relatively unstable. In particular, χ^2 oscillated between values of 1.44 and 1.56 due to excessive correlations between the occupancies of the Ag^+ sites, their thermal vibration parameters and (to a lesser extent) their positional parameters. Since reliable values of the occupancies of the various Ag^+ sites is essential to investigate the probable diffusion pathways adopted by the cations we take the final refined values (listed in Table 1) to be those obtained with anisotropic thermal vibrations for Rb, I1 and I2 and isotropic thermal vibrations for all the Ag^+ sites. The difficulties in describing the rather broad and irregular time-averaged distributions of Ag^+ within such compounds has been discussed previously (10) and is a recurring problem in deriving structural descriptions of superionic compounds. More complex models, describing the thermal vibrations by including anharmonic effects, involve the use of many additional fitted parameters and are probably only appropriate to single-crystal studies. In the case of the powder diffraction data presented here, we instead adopt a Maximum Entropy (MaxEnt) Fourier difference method to generate graphical descriptions of the most probable Ag^+ density within the unit cell, in a manner which incorporates the inherent limitations of the powder method such as peak overlap, etc. This will be discussed in the following section. The positional parameters listed in Table 1 are found to agree within ~ 3 e.s.d. with those

TABLE 1

Summary of the Results of the Least-Squares Refinements of the Neutron Diffraction Data Collected from $RbAg_4I_5$, KAg_4I_5, and KCu_4I_5

		$RbAg_4I_5$	KAg_4I_5	KCu_4I_5
Temperature	T(K)	298(2)	348(4)	584(5)
Lattice parameter	a (Å)	11.23934(3)	11.15827(4)	10.87195(11)

TABLE 1—*Continued*

		$RbAg_4I_5$	KAg_4I_5	KCu_4I_5
Rb/K in 4(*a*)	x	$\frac{3}{8}$	$\frac{3}{8}$	$\frac{3}{8}$
	y	$\frac{3}{8}$	$\frac{3}{8}$	$\frac{3}{8}$
	z	$\frac{3}{8}$	$\frac{3}{8}$	$\frac{3}{8}$
	B_{11} (Å^2)	9.4(2)	8.4(2)	
	B_{12} (Å^2)	−4.5(1)	−3.7(2)	$B_{iso} = 15.1(9)$
	B_{Equiv} (Å^2)	7.6(2)	7.2(2)	
I1 in 8(*c*)	x	0.0307(2)	0.0377(2)	0.0431(5)
	y	$= x$	$= x$	$= x$
	z	$= x$	$= x$	$= x$
	B_{11} (Å^2)	4.17(8)	5.02(7)	
	B_{12} (Å^2)	0.08(8)	0.11(6)	$B_{iso} = 4.8(2)$
	B_{Equiv} (Å^2)	4.14(9)	4.98(8)	
I2 in 12(*d*)	x	$\frac{1}{8}$	$\frac{1}{8}$	$\frac{1}{8}$
	y	0.1773(1)	0.1873(2)	0.1504(4)
	z	$\frac{1}{4} + y$	$\frac{1}{4} + y$	$\frac{1}{4} + y$
	B_{11} (Å^2)	4.2(2)	4.9(2)	
	B_{12} (Å^2)	5.3(1)	6.0(2)	
	B_{12} (Å^2)	0.6(1)	0.5(1)	$B_{iso} = 5.1(2)$
	B_{23} (Å^2)	−0.7(1)	−0.2(1)	
	B_{Equiv} (Å^2)	4.2(2)	5.0(2)	
Ag1/Cu1 in 24(*e*)	x	0.5293(5)	0.5357(7)	0.5343(12)
	y	0.2707(4)	0.2601(6)	0.2728(11)
	z	0.7992(5)	0.7904(6)	0.8006(12)
	B_{iso} (Å^2)	7.4(2)	9.8(3)	9.2(6)
	m	9.5(1)	9.3(1)	9.0(5)
Ag2/Cu2 in 24(*e*)	x	0.9960(8)	0.9883(8)	0.992(3)
	y	0.8535(8)	0.8571(9)	0.859(3)
	z	0.2140(9)	0.2142(12)	0.223(3)
	B_{iso} (Å^2)	8.0(4)	9.3(4)	15(2)
	m	6.1(2)	6.4(1)	6.0(5)
Ag3/Cu3 in 8(*c*)	x	0.175(1)	—	0.173(2)
	y	$= x$	—	$= x$
	z	$= x$	—	$= x$
	B_{iso} (Å^2)	4.6(11)	—	6(2)
	m	0.4(2)	0 (fixed)	1.0(6)
R-factors	R_W (%)	0.53	0.67	0.61
	R_{exp} (%)	0.43	0.52	0.58
	R_{Bragg} (%)	0.26	0.31	0.34
No. of data points	N_d	2944	2876	2265
No. of peaks	N_p	243	256	113
No. of variables	N_v	38	37	33

Note. B_{ij} are the components of the anisotropic thermal vibrations (defined by $B_{ij} = 8^2\langle u_{ij}^2\rangle$, where u_{ij} is the mean-square amplitude of the vibration in direction ij). B_{Equiv} is the equivalent isotropic thermal vibration parameter in those cases where anisotropic thermal vibrations have been refined and B_{iso} is the refined isotropic thermal vibration parameter. The weighted and expected *R*-factors are given by $R_W^2 = \sum_{N_d}(y_{obs} - y_{calc})^2/(\sigma y_{obs})^2/\sum_{N_d}(y_{obs})^2/(\sigma y_{obs})^2$ and $R_{exp}^2 = (N_d - N_v)/\sum_{i=1}^{N_d}(y_{obs})^2/(\sigma y_{obs})^2$ and the summations are made over the N_d data points used in the fit. N_v is the number of fitted variables. y_{obs} and y_{calc} are the observed and calculated intensities, respectively, and σy_{obs} is the estimated standard deviation on y_{obs} derived from the counting statistics. The Bragg *R*-factor is given by $R_{Bragg}^2 = \sum_{N_p}(I_{obs} - I_{calc})^2/(\sigma I_{obs})^2/\sum_{N_p}(I_{obs})^2/(\sigma I_{obs})^2$ where the N_p Bragg peaks have observed and calculated intensities I_{obs} and I_{calc}, respectively, and σI_{obs} is the estimated standard deviation on I_{obs}.

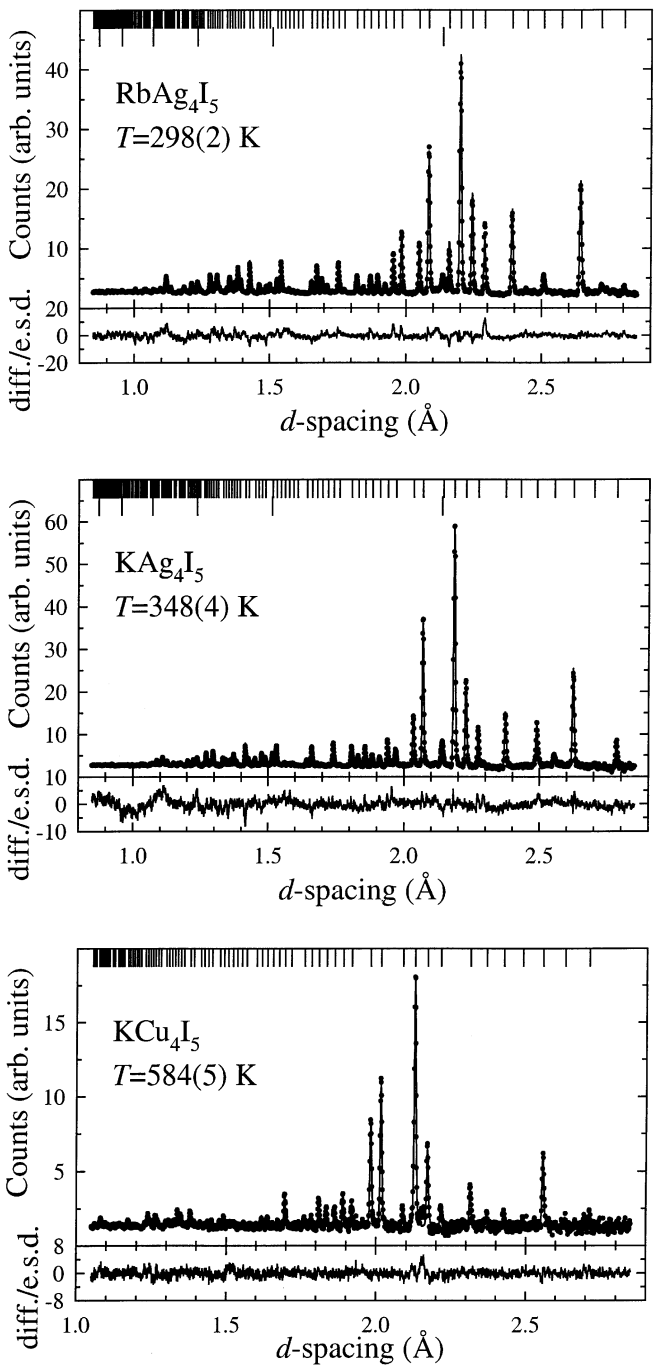

FIG. 3. The least-squares fit to the powder neutron diffraction data collected from $RbAg_4I_5$ at 298(2) K (top), KAg_4I_5 at 348(4) K (middle) and KCu_4I_5 at 584(5) K (bottom). The dots are the experimental data points (with fitted background subtracted) and the solid line is the calculated profile using the parameters listed in Table 1. The lower trace shows the difference (measured minus calculated) divided by the estimated standard deviation on the experimental data points. The upper row of tick marks along the top of the figure denote the calculated positions of all the symmetry allowed Bragg reflections. For $RbAg_4I_5$ and KAg_4I_5, the lower row of ticks denote the positions of weak additional reflections arising from the vanadium sample container which are also included in the fit.

published by Geller (9) on the basis of single-crystal X-ray diffraction. The occupancies of the Ag1 sites are also in agreement, though we find a slightly higher proportion of cations on the Ag2 sites at the expense of any occupancy of the Ag4 positions. The quality of the fit to the diffraction data is shown in Fig. 3.

We now consider the KAg_4I_5 and KCu_4I_5 data collected at $T = 348(4)$ and 584(5) K, respectively. In both cases, the observed diffraction peaks could be successfully accounted for using cubic unit cells with $a \sim 11.16$ and 10.87 Å, respectively. The measured reflections indicate the presence of only a single condition $h = 4n$ on $h00$ type peaks, which is consistent with $P4_132$ symmetry. Model-independent fits to both datasets confirmed this assignment in both cases, with $\chi^2 = 1.44$ and 1.08, respectively. Refinements of the structural model began with the final arrangement derived for $RbAg_4I_5$ above. In the case of KAg_4I_5, no significant occupancy of the Ag3 site was found and a non-physical (negative) value of its isotropic thermal vibration parameter was found. As a consequence, the Ag3 site was excluded from the fitting procedure for this compound. In the case of KCu_4I_5, no significant improvement occurred when allowing K, I1 and I2 ions to have anisotropic thermal vibrations and these were constrained to be isotropic. The final fits gave χ^2 values of 1.62 and 1.11 for KAg_4I_5 and KCu_4I_5, respectively, with the parameters listed in Table 1. In general, the values obtained for KCu_4I_5 have e.s.d.'s around three times higher than those for the two Ag^+ compounds. This is a consequence of the higher temperature of measurement (because the greater thermal vibrations lead to a more rapid fall-off in intensity at lower d-spacings) and the increased background level due to the silica ampoule used to encapsulate the sample. The fits to the diffraction data for KAg_4I_5 and KCu_4I_5 are illustrated in Fig. 3.

4. DISCUSSION

In developing a structural description for the three MA_4I_5 phases discussed in the previous section, we initially consider the nature of the I^- sublattice. The structures of the three phases are sufficiently similar that, in providing details of the interionic distances, etc., it is only necessary to quote the values for one example. $RbAg_4I_5$ is chosen for this purpose.

As discussed previously (9), the anion sublattice within $RbAg_4I_5$ adopts the so-called β-Mn structure, which is the arrangement of the atoms in elemental manganese in the temperature range 1000–1368 K. The Mn1 and Mn2 sites in β-Mn (which are equivalent to the I1 (8(c) x,x,x) and I2 (12(d) $\frac{1}{8},y,\frac{1}{4}-y$) positions described in the previous section) have values $x_{Mn1} = 0.0636(1)$ and $y_{Mn2} = 0.2022(1)$ (24), these being very close to the ideal values obtained if the shortest Mn2–Mn2 and Mn1–Mn2 distances are made equal ($x_{Mn1} = 1/(9 + \sqrt{33}) = 0.0678$ and $y_{Mn2} = (9 - \sqrt{33})/$

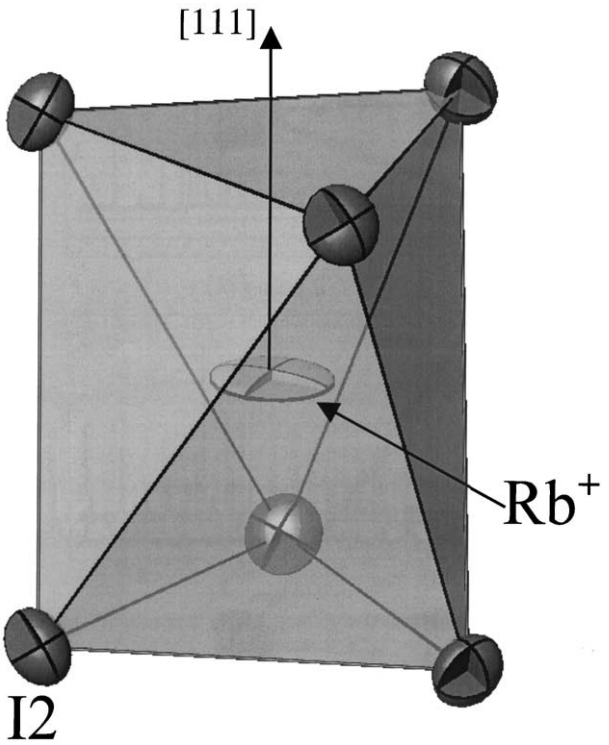

FIG. 4. The distorted octahedral environment of $6 \times$ I2 anions around Rb^+ in $RbAg_4I_5$. The highly anisotropic nature of the thermal vibrations of the Rb^+ is illustrated.

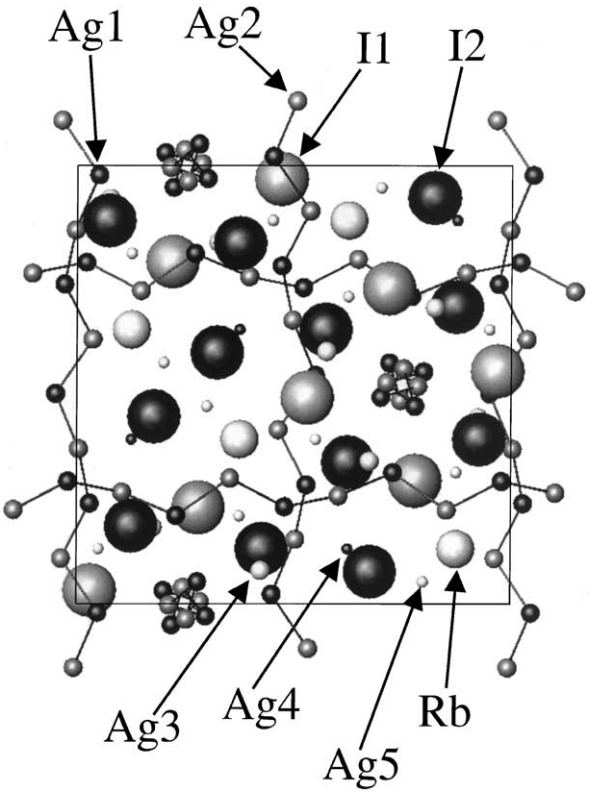

FIG. 5. The crystal structure of $RbAg_4I_5$, showing the cubic unit cell as the narrow-lined box. The larger spheres denote I1 (gray) and I2 (black) and Rb^+ (white). The five proposed sites for Ag^+ are illustrated as smaller spheres. Those found to be significantly occupied in this work are shown as Ag1 (black), Ag2 (gray) and Ag3 (white). The bold lines indicate the infinite non-intersecting Ag1Ag2Ag1 ... strings parallel to each of the cubic axes described in the text. The two unoccupied sites Ag4 and Ag5 are shown as very small black and white spheres, respectively.

$16 = 0.2035$ (25)). The corresponding values for x_{I1} and y_{I2} in $RbAg_4I_5$ (Table 1) indicate that the I^- sublattice is somewhat distorted by the introduction of the two cation species. Each I1 anion is surrounded by $3 \times$ I1 at 4.504 Å and a further $9 \times$ I2 in the range 4.366–4.869 Å, whilst each I2 anion is surrounded by $10 \times$ I1 in the distance range 4.366–4.869 Å.

Within the anion sublattice, there are only four distorted octahedral cavities, which are the 4(*a*) $\frac{3}{8},\frac{3}{8},\frac{3}{8}$ sites occupied by the Rb^+ in $RbAg_4I_5$. The nature of this distortion is illustrated in Fig. 4. If viewed down the three-fold axis the opposite triangular faces are twisted with respect to one another, such that the six Rb–I2 distances remain equal (3.630 Å) but the polyhedron is intermediate between a trigonal prism and an octahedron. The highly anisotropic nature of the Rb^+ thermal vibrations is evident in Fig. 4. Nuclear Quadrupole Resonance studies (11) indicate that the site symmetry of the Rb^+ in $RbAg_4I_5$ is lower than the 32 suggested by diffraction methods, implying that the thermal vibration ellipsoid is modelling some local static disorder involving small displacements away from the three-fold axis. However, attempts to model such behavior using fractionally occupied "split sites" was not successful.

There are three relatively regular tetrahedral cavities, two in 24(*e*) sites and one in 8(*c*). These correspond to the Ag1, Ag2 and Ag3 sites discussed above. The Ag1 site is surrounded by $2 \times$ I1 and $2 \times$ I2 in the distance range 2.825–2.939 Å, the Ag2 by $2 \times$ I1 and $2 \times$ I2 in the distance range 2.744–2.892 Å and the Ag3 by $1 \times$ I1 and $3 \times$ I2 at 2.809–2.891 Å. The (unoccupied) Ag4 and Ag5 sites are at the centers of a five-fold cavity formed by $2 \times$ I1 and $3 \times$ I2 at 3.031–3.143 Å and a heavily distorted tetrahedron of $2 \times$ I1 at 2.810 Å and $2 \times$ I2 at 3.141 Å. The locations of these sites are shown in Fig. 5.

As demonstrated by Fig. 5, the β-Mn structure has proved difficult to describe simply (25, 26). O'Keeffe and Andersson (25) considered the structure to be comprised of identical infinite cylinders parallel to the $\langle 111 \rangle$ directions comprising a repeating sequence of distorted $I2_6$ polyhedra and four $I1I2_3$ tetrahedra. An alternative description by Nyman *et al.* (26) considered infinite strings of $I1_2I2_2$ tetrahedra coincident with the 4_1 axes, such that there are two such strings running parallel to each of the three $\langle 100 \rangle$ axes which do not intersect. These tetrahedra are alternatively

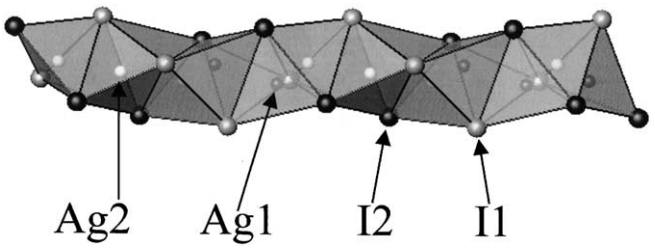

FIG. 6. The infinite strings of face-sharing anion tetrahedra formed around the Ag1Ag2Ag1 … strings of cation sites in $RbAg_4I_5$. The larger spheres are I1 (gray) and I2 (black) anions, whilst the smaller ones denote Ag1 (black) and Ag2 (gray) sites.

occupied by the Ag1 and Ag2 sites and share faces in the manner shown in Fig. 6. This is further illustrated in Fig. 5 by the joining of the Ag1 and Ag2 sites to show how these infinite strings are arranged within the three-dimensional lattice. Given the predominant occupancy of the Ag1 and Ag2 sites determined by the least-squares refinement of the neutron diffraction data for all three MA_4I_5 phases, it is reasonable to conclude that these represent significant diffusion pathways for the Ag^+. Thus, migration occurs predominantly in one-dimensional channels between sites characterized by close to ideal tetrahedral co-ordination, giving rise to the high observed ionic conductivity (Fig. 1).

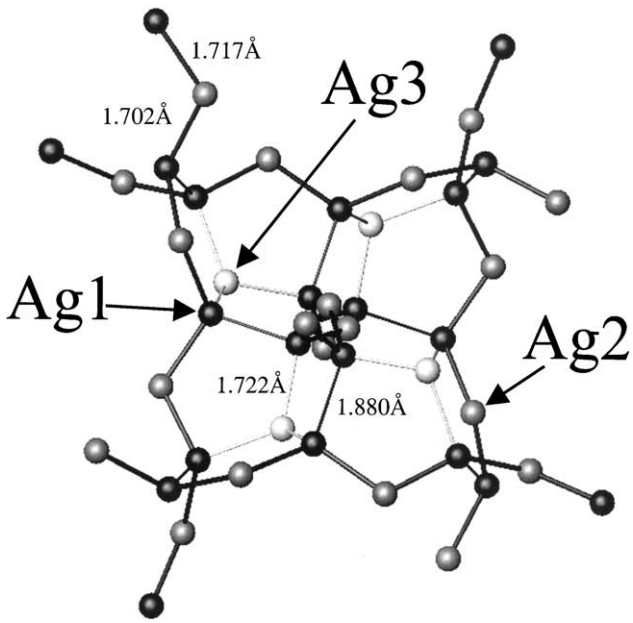

FIG. 7. Possible conduction pathways within $RbAg_4I_5$. For clarity, the I^- and Rb^+ are not illustrated, their positions can be established by reference to Fig. 5. The Ag1Ag2Ag1 … strings parallel to each of the cubic axes can be joined directly at the Ag1 sites or indirectly via the Ag3 positions.

Clearly, a question which arises from this simple picture of the Ag^+ conduction mechanism is the extent to which the cations migrate between different channels. On geometric grounds, there are two plausible routes for this to occur, which are illustrated in Fig. 7. When viewed down one of the principal cubic directions the Ag1Ag2Ag1 … strings cross where there are two Ag1 sites a distance 1.880 Å apart. Since this is only marginally longer than the Ag1–Ag2 distances within the channels (1.702 and 1.717 Å), direct hopping between the channels might occur. Alternatively, Ag^+ transfer between the two channels could occur via the Ag3 sites (see Fig. 7). The Ag3 sites lie at the center of a regular tetrahedron of I^- (see above), and are thus favorable sites for Ag^+, whilst the Ag1–Ag3 distances are only 1.772 Å. Unfortunately, the difficulty in obtaining a reliable value for the occupancy of the Ag3 site from the least-squares refinements (previous section) make it difficult to assess the relative merit of these two proposed schemes.

As discussed above, it can be difficult to parameterize the extensive thermal vibrations of ions within superionic compounds reliably, since these cause a rapid fall-off in the intensity of the Bragg peaks at low *d*-spacings. In addition, the Bragg intensities are often superimposed on an undulating diffuse scattering background (making it difficult to extract the intensities) and (in the case of powder diffraction) there is inevitably a degree of peak overlap. These circumstances, combined with the presence of partially occupied sites, make it difficult to obtain an unambiguous characterization of the superionic phase in terms of ionic positions, site occupancies and complex thermal vibration parameters, without the risk of overanalyzing the data. As a result, we adopt a more general approach and use a MaxEnt analysis to determine the location of the Ag^+ within the sublattice formed by the I^- and Rb^+, in a manner analogous to the solution of crystal structures using a known fragment (the Heavy Atom method). This novel approach (27) uses the MemSys package (Maximum Entropy Data Consultants Ltd., Cambridge, UK) and is particularly powerful for powder diffraction studies, since the use of probability theory includes both the phase and amplitude information contained in the "known" part of the structure and the use of a covariance matrix describing the correlations between the extracted intensities of neighboring reflections allows all the information from overlapped reflections to be taken into account. In addition, it is possible to include prior information such as the overall positivity of the scattering density distribution (which is true for the compounds considered here, since the scattering lengths of all the constituent ions are positive) and its smoothness on a local scale in a statistically rigorous manner. Put simply, the MaxEnt formulation makes full use of the information content contained in the diffraction pattern and, in practical terms, is less prone to excessive termination ripples which are an inevitable consequence of "normal" Fourier methods.

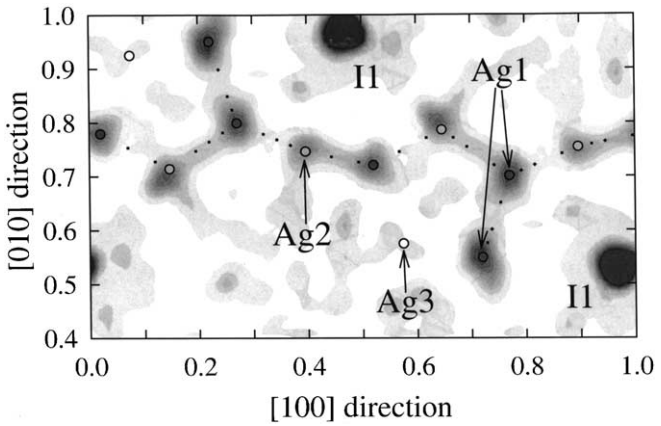

FIG. 8. MaxEnt reconstruction of the scattering (ionic) density within $RbAg_4I_5$. The (001) section shown is a slice with $0.45 \leq z \leq 0.55$. The conduction along one of the Ag1Ag2Ag1 … strings is shown by the dotted line at $y \sim \frac{3}{4}$. The density between the Ag1 sites (at, for example, 0.72, 0.55, 0.52 and 0.77, 0.70, 0.47) indicates that Ag^+ may hop between the channels via this route. The Ag3 site does not appear to be a significant conduction pathway.

Figure 8 shows the MaxEnt reconstruction (model + difference) obtained using the diffraction data collected from $RbAg_4I_5$ at ambient temperature. All possible reflections have been used, including those at long d-spacings collected in detector banks at lower scattering angles (19). The section shown is viewed down the 001 axis and is a section of the scattering density with $0.45 \leq z \leq 0.55$. The two I1 positions at approximately (0.47, 0.97, 0.53) and (0.97, 0.53, 0.47) are clearly visible and the channel of alternate Ag1 and Ag2 sites along the [100] direction at $y \sim \frac{3}{4}$ is shown. Some spread of scattering density (Ag^+ distribution) between the sites can be seen, indicative of diffusion along these pathways as discussed above. Of particular interest is the distribution of Ag^+ between the two Ag1 sites, which corresponds to direct hopping between the channels (the peaks at approximately (0.22, 0.95, 0.48) and (0.72, 0.55, 0.52) represent Ag1 sites which form part of channels running out of the plane of the paper, as shown in Fig. 5). There appears to be no significant density at the Ag3 site, or between the Ag3 and its two neighboring Ag1 sites. We therefore conclude that the dominant Ag^+ diffusion in $RbAg_4I_5$ is hopping between the Ag1 and Ag2 sites along the channels parallel to the $\langle 001 \rangle$ directions, with exchange of Ag^+ between these channels taking place between Ag1 sites. Maximum entropy reconstructions using the diffraction data collected for KAg_4I_5 and KCu_4I_5 showed similar cation distributions, though in the latter case the peaks at the Cu1 and Cu2 sites are less well pronounced. This is presumably a consequence of the higher measurement temperature resulting in more extensive thermal vibrations of the cations and more rapid diffusion of the Cu^+.

5. CONCLUSIONS

The superionic behavior of the three compounds $RbAg_4I_5$, KAg_4I_5 and KCu_4I_5 has been investigated. Their crystal structures and, in particular, the distribution of the mobile cations are found to be very similar, suggesting that the properties of both the mobile and immobile cation species play a relatively minor role in the diffusion process. This is supported by the relatively similar values of their ionic conductivities. Detailed information concerning the likely conduction pathways has been provided by the application of a MaxEnt difference Fourier method to examine the distribution of Ag^+/Cu^+ within the unit cell. This approach may prove valuable in the study of other superionic phases, where the modelling of rather broad and irregular-shaped peaks in the ionic density distribution cannot be reliably described using "traditional" isotropic and anisotropic models for the thermal vibrations of ions on well-defined sites (especially, if these are only fractionally occupied). Whilst the application of anharmonic models of the thermal vibrations can be used (10), their application is likely to be limited to single-crystal studies, due to the inherently smaller number of reflections that are typically obtained by powder methods. In general, it should be emphasized that the MaxEnt method described here should not be used as a substitute for collecting data with the highest possible $\Delta d/d$ resolution. However, in those cases where the inevitable experimental trade-off in intensity (as in the case of the significant neutron absorption in the Ag^+ compounds considered here) or d-spacing range prohibit the collection of ultra-high-resolution data in a feasible time scale its applications look promising. Of course, details of the conduction mechanisms are only *inferred* from such studies, since Bragg diffraction data contains information on the *time-averaged* ionic distribution within the unit cell. Analysis of the diffuse scattering (to probe the short-range correlations between disordered ions) and molecular dynamics simulations (to investigate the Ag^+ hopping rate and geometry) are underway to provide further insight into the behavior of these interesting compounds.

ACKNOWLEDGMENTS

The work presented in this paper forms part of a wider project investigating the structural properties of superionic conductors funded by the Engineering and Physical Sciences Research Council (reference GR/M38711). One of the authors (PB) thanks the Swedish Research Council for financial support. We are grateful to J. Dreyer for assistance with the high-temperature neutron-diffraction measurements.

REFERENCES

1. J. N. Bradley and P. D. Greene, *Trans. Faraday Soc.* **62,** 2069 (1966).
2. J. N. Bradley and P. D. Greene, *Trans. Faraday Soc.* **63,** 424 (1967).

3. O. Yamamoto, *in* "Fast-Ion Transport in Solids" (B. Scrosati, A. Magistris, C. M. Mori, and G. Mariotto, Eds.), NATO ASI Series, Vol. E, 250, p. 203. Kluwer Academic Publishers, Dordrecht, 1993.
4. A. Wojakowska, E. Krzyak, and A. Wojakowski, *Thermochim. Acta* **344,** 55 (2000).
5. S. E. Rao and R. C. Bhuniya, *J. Mater. Sci. Lett.* **3,** 221 (1984).
6. S. Geller, J. R. Akridge, and S. A. Wilber, *Phys. Rev. B* **19,** 5396 (1979).
7. R. Kanno, K. Ohno, Y. Kawamoto, Y. Takeda, O. Yamamoto, T. Kamiyama, H. Asano, F. Izumi, and S. Kondo, *J. Solid State Chem.* **102,** 79 (1993).
8. J. N. Bradley and P. D. Greene, *Trans. Faraday Soc.* **63,** 2516 (1967).
9. S. Geller, *Science* **157,** 310 (1967).
10. W. F. Kuhs, *Acta Crystallogr. A* **39,** 148 (1983).
11. D. Brinkmann, W. Freudenreich, H. Arend, and J. Roos, *Solid State Comm.* **27,** 133 (1978).
12. C. García, J. I. Franco, J. C. López Tonazzi, and N. E. Walsöe de Reca, *Solid State Ionics* **9–10,** 1233 (1983).
13. T. Sakuma, T. Aoyama, and H. Takahashi, *Solid State Ionics* **79,** 71 (1995).
14. M. Pasternak, *Phys. Rev. B* **28,** 82 (1983).
15. P. C. Allen and D. Lazarus, *Phys. Rev. B* **17,** 1913 (1978).
16. D. Wilmer, K. Funke, T. Kloidt, and C. J. Carlile, *Ber. Bunsenges. Phys. Chem.* **95,** 1137 (1991).
17. K. Funke, T. Kloidt, D. Wilmer, and C. J. Carlile, *Solid State Ionics* **53–56,** 947 (1992).
18. S. Geller, *Phys. Rev. B* **14,** 4345 (1976).
19. S. Hull, R. I. Smith, W. I. F. David, A. C. Hannon, J. Mayers, and R. Cywinski, *Physica B* **180&181,** 1000 (1992).
20. W. I. F. David, R. M. Ibberson, and J. C. Matthewman, *Rutherford Appleton Laboratory Report* RAL-92-032, 1992.
21. P. J. Brown and J. C. Matthewman, *Rutherford Appleton Laboratory Report* RAL-87-010, 1987.
22. N. J. G. Gardner, S. Hull, D. A. Keen, and P. Berastegui, *Rutherford Appleton Laboratory Report* RAL-TR-1998-032, 1998.
23. G. S. Pawley, *J. Appl. Crystallogr.* **14,** 357 (1981).
24. C. B. Shoemaker, D. P. Shoemaker, T. E. Hopkins, and S. Yindepit, *Acta Crystallogr. B* **34,** 3573 (1978).
25. M. O'Keeffe and S. Andersson, *Acta Crystallogr. A* **33,** 914 (1977).
26. H. Nyman, C. E. Carroll, and B. G. Hyde, *Z. Kristallogr.* **196,** 39 (1991).
27. D. S. Sivia and W. I. F. David, *J. Phys. Chem. Solids* **62,** 2119 (2001).